HHS Public Access

Author manuscript

Drug Deliv Transl Res. Author manuscript; available in PMC 2017 June 16.

Published in final edited form as:

Drug Deliv Transl Res. 2016 April ; 6(2): 96–104. doi:10.1007/s13346-015-0244-0.

Enhanced osseous integration of human trabecular allografts following surface modification with bioactive lipids

Tiffany Wang[1], **Jack Krieger**[1], **Cynthia Huang**[2], **Anusuya Das**[2], **Michael P. Francis**[3], **Roy Ogle**[4], and **Edward Botchwey**[1]

[1]Wallace H. Coulter Department of Biomedical Engineering, Georgia Institute of Technology and Emory University, 315 Ferst Drive Rm 1311, Atlanta, GA 30332, USA

[2]Department of Biomedical Engineering, University of Virginia, Charlottesville, VA 22903, USA

[3]LifeNet Health, Virginia Beach, VA 23453, USA

[4]School of Medical Diagnostic and Translational Science, Old Dominion University, Norfolk, VA 23529, USA

Abstract

In this study, we used extracellular matrix (ECM) gels and human bone allograft as matrix vehicles to deliver the sphingolipid growth factor FTY720 to rodent models of tibial fracture and a critical-sized cranial defect. We show that FTY720 released from injectable ECM gels may accelerate callous formation and resolution and bone volume in a mouse tibial fracture model. We then show that FTY720 binds directly to human trabecular allograft bone and releases over 1 week in vitro. Rat critical-sized cranial defects treated with FTY720-coated grafts show increases in vascularization and bone deposition, with histological and micro-computed topography (microCT) evidence of enhanced bone formation within the graft and defect void. Immunohistochemical analysis suggests that osteogenesis within FTY720-coated grafts is associated with reduced $CD68^+$ macrophage infiltration and recruitment of $CD29^+$ bone progenitor cells. Matrix binding of FTY720 thus represents a promising and robust bone regeneration strategy with potential clinical translatability.

Keywords

Bone allograft; Sphingosine 1-phosphate; FTY720; Extracellular matrix; Regeneration

Correspondence to: Edward Botchwey.

Tiffany Wang and Jack Krieger contributed equally to this work.

Conflict of interest T.W., J.K., C.H., A.D., R.O., and E.B. declare that they have no conflict of interest. M.P.F. is an employee of LifeNet Health.

Ethical standards and animal care Experiments comply with the current laws of the USA. All institutional and national guidelines for the care and use of laboratory animals were followed.

Introduction

Treatment of musculoskeletal injuries carries an estimated annual burden of $127 billion in the USA [1], of which $2.5 billion annually is spent on an average of 1.5 million autograft or allograft procedures [2]. The current gold standard of bone graft treatment, using autologous bone harvested from the iliac crest [3], often is of insufficient mass to successfully repair the bone defect, with the secondary operation to obtain this tissue often causing donor site pain and morbidity [3, 4]. To meet the growing clinical need for bone reconstruction material and overcome the limited supply of autografts, bone allografts from donors have been used extensively to repair bone wounds. However, massive transplants using allografts experience a 30–60 % failure rate [5] and lose 50 % of their strength after 10 years [6]. Since vascularization and new bone formation are critical for stable incorporation of massive allografts, for example in large skull flaps commonly transplanted in wounded soldiers, there is a clinical need for new grafting technologies that enhance these endogenous reparative processes. In addition to annual costs of grafting procedures, $120 billion is spent to treat bone injuries that do not necessitate grafts, including 7.9 million annual bone fractures that carry a 10 % incidence of non-union [7], which leads to improper healing and higher risk of re-injury. The development of an off-the-shelf acellular therapy that could meet both graft-based and graft-independent treatment of bone defects is clinically desirable.

Previously, we have demonstrated enhanced angiogenesis and regeneration in multiple injury models via local delivery of small molecules, particularly FTY720, a synthetic analog of sphingosine 1-phosphate (S1P) with agonist activity at S1P receptors $S1P_1$ and $S1P_{3–5}$ [8–14]. Oral administration of FTY720 is approved by the FDA to treat relapsing-remitting multiple sclerosis, with the predominant mechanism being sequestration of lymphocytes in secondary lymph organs [15]. We have shown that sustained release of FTY720 from poly(lactic-co-glycolic-acid) (PLAGA)-based scaffolds promotes osseous regeneration and vascularization within critical-sized bone defects [10–13, 16]. PLAGA is a widely used synthetic material for medical applications [17–20]. Despite extensive literature applying PLAGA in animal models, and its status as a FDA-approved material, a small fraction of PLAGA-based technologies have progressed to clinical trials and only a select few are commercially available. One potential concern with using PLAGA is that its degradation on the nanoscale level may be more toxic than on the microscale level [21].

Incorporating natural extracellular matrix (ECM) into biomaterial systems provides relevant biochemical and biophysical guidance cues to direct regeneration in bone, cartilage, nerve, and cardiac tissue [22–26]. Additionally, it is now a common practice in tissue engineering to exploit the capability of ECM to sequester and release tissue morphogens, but there are few strategies in the literature utilizing ECM to achieve controlled release of hydrophobic small molecules [27–29]. In the present study, we locally deliver FTY720 from ECM gel and human trabecular bone allograft to promote healing in models of endochondral and intramembranous bone regeneration, respectively. We show for the first time that FTY720 may accelerate fracture healing when released from an injectable murine basement membrane–based hydrogel (Matrigel®) plug in a murine tibial fracture model. We then show that FTY720 can adsorb to and release from the surface of devitalized human allograft bone matrix over 1 week in vitro. Direct coating of human trabecular bone grafts with

FTY720 accelerates new bone deposition in a rat critical-sized cranial defect model, possibly due to accelerated vascularization, decreased recruitment of macrophages, and increased recruitment of bone progenitors.

Materials and methods

Welfare of animals

Animals were procured from Charles River Laboratories International (Wilmington, MA), and all applicable international, national, and institutional guidelines for the care and use of animals were followed. All procedures performed in studies involving animals were in accordance with the ethical standards of the University of Virginia Animal Care and Use Committee.

Mouse tibial fracture model

Male BALB/c mice aged 10 weeks and weighing 20–25 g were anesthetized via intraperitoneal (i.p.) injections of ketamine (100 mg/kg) and xylazine (10 mg/kg) in saline. A sterile metal pin was inserted into the medullary canal to provide mechanical stability in the leg, and a fracture was created in the tibia using a Bonnarens-Einheron appartus as the impact device, where a 220-g weight was dropped from a height of 40 cm onto a blunt blade in contact with the tibia. Animals were treated with local injections of 0.1 mL Matrigel® (BD Biosciences, San Jose, CA), or Matrigel® containing low (1 nM) and high (10 nM) doses of FTY720 (Cayman Chemical, Ann Arbor, MI) which self-assembled into hydrogel plugs within the defect space at body temperature. Because the intramedullary metal pin interfered with micro-computed tomography (microCT) imaging, X-ray images were acquired weekly to track bone regeneration in the mouse tibial defect. Each week, mice were anesthetized via i.p. injections of ketamine (100 mg/kg) and xylazine (10 mg/kg) in saline and imaged using X-ray (exposure time=1 min at 30 eV). For microCT assessment of bone density and volume, mice were euthanized by CO_2 asphyxiation and their tibias were harvested at week 2 (n=3) and week 4 (n=3). The pin was removed, and the bone volume and bone density of the entire tibia were imaged using a VivaCT40 Scanner (SCANCO Medical, Brutusellen, Switzerland) at medium resolution using a voxel dimension of 21 μm. Tibia were embedded in paraffin and sections were prepared for hematoxylin and eosin (H&E) staining according to standard protocols.

Drug binding to hydroxyapatite

Surface adsorption of FTY720 to hydroxyapatite was visualized using fluorescent NBD-FTY720. Briefly, fragments of hydroxyapatite (3D Biotek, Hillsborough, NJ) were immersed in 10 μg/500 μL NBD-FTY720 (Cayman Chemical, Ann Arbor, MI) in methanol for 2 h and then rinsed once with PBS. Coated fragments were imaged using a Zeiss 710 NLO confocal microscope at 488-nm excitation and ×5 magnification (Zeiss, Thornwood, NY).

Drug release from human trabecular bone grafts

Allografts from research-consented donor were processed at LifeNet Health (Virginia Beach, VA). The mineralized cancellous bone allografts were processed with LifeNet's

clinically proven Allowash XG® technology to remove >99 % of bone marrow and blood elements from the bone matrix, and also rendering the material sterile while maintaining biomechanical and biochemical properties. Processed allografts were received in the form of discs (8-mm radius, 1-mm thickness) and then cut in half into semicircular shape. For direct adsorption, bone grafts were gently vortexed for 4 h in a solution of 1.5 mg/0.6 mL FTY720 in methanol, or methanol only for control grafts. All bones were kept at 4 °C for 24 h to dry and then lyophilized for 24 h to extract remaining solvent (Labconco Corp., Kansas City MO). The pre-loading and post-loading solutions were saved to measure FTY720 content in order to determine drug loading efficiency. For in vitro release, grafts were placed in vials containing 1 mL simulated body fluid (pH 7.2; 7.996 g NaCl, 0.35 g $NaHCO_3$, 0.3 g KCl, 0.13 g KH_2PO_4, 0.095 g $MgCl_2$, 0.278 g $CaCl_2$, 0.06 g $MgSO_4$ in 1 L deionized water; all salts from Sigma-Aldrich, St. Louis, MO) with 4 % (*w*/*v*) fatty acid free bovine serum albumin (FAF-BSA) and maintained at 37 °C with constant agitation. Each day, the bone was moved to a new vial with fresh solution. The solutions were taken through sphingolipid extraction, and sphingolipid content was measured using a Shimadzu UFLC High Performance Liquid Chromatograph (Columbia, MD) equipped with a Supelco Discovery C18, 5 μm connected to an ABI 4000 QTrap quadruple mass spectrometer (Applied Biosystems, USA). Briefly, D-*erythro*−Sphingosine (C-17 base) internal standard was added to each sample, sonicated for 10 min, and immediately incubated at 48 °C for 16 h. After cooling to room temperature, KOH (0.2 mL, 1 M) was added and the solution was centrifuged at 10,000*g* for 10 min at 4 °C. The supernatant was collected and dried to solid with nitrogen air flow and stored at −20 °C. Immediately before running the sample on the HPLC, the extraction residue was dissolved in methanol (0.3 mL) and centrifuged at 12,000*g* for 12 min at 4 °C.

Rat cranial defect model

Female Sprague–Dawley rats aged 6–8 weeks and weighing ≈235 g underwent a critical-sized (8 mm) cranial defect surgery [12]. Briefly, animals were anesthetized via i.p. injection of ketamine (80 mg/kg) and xylazine (8 mg/kg) in saline. The dorsal skin was sterilized and a longitudinal incision was made over the dorsum of the skull over the sagittal suture through the skin and periosteum. The periosteum was elevated and reflected laterally. A 3-mm round burr was used to create a 8-mm defect in the bone under constant saline irrigation using a Hall High Speed Drill (CONMED, Linvatec, Largo, FL). The semicircular graft was placed underneath the periosteum, in direct contact with the parietal bone, centered on the sagittal suture and between the coronal and lamboid sutures. The periosteum and skin were sutured shut, and animals were given Ketoprofen (3 mg/kg SC) for 3 days as a post-operative analgesic. Rats were given free access to food and water and were monitored for complications or abnormalities. The animals received one of three treatments: no implant (empty defect), human trabecular semicircular bone graft (graft only), and FTY720-coated human trabecular semicircular bone graft (graft + FTY720). FTY720 was adsorbed directly to the bone grafts as previously described. Grafts were analyzed and distributed evenly across the two graft groups to control for graft size and density variation.

MicroCT analysis of the cranial defect

Rats were anesthetized via 2.5 % isoflurane gas and quantitatively analyzed for bone volume and bone density at weeks 0, 2, 4, 6, 10, and 12 (n=3 per time point). Scanning parameters in air were as follows: 38-μm voxel size, 55 kVp, 145 μA, medium resolution, 38.9-mm-diameter field of view, and 200-ms integration time (73-mGy radiation per scan). The threshold for bone evaluation was set at 481.3 mg hydroxyapatite (HA)/cm^3. All scans maintained the same number of slices (≈260 slices) for the entire study, centered at the defect, with equal extension in the anterior and posterior directions from the edges of the defect. Regions of interest were drawn on the 2D image slices. In the cranial defect, the circular region of interest was bound by the physiological ridges that separate the parietal bone from the temporal bone, resulting in the inclusion of all the parietal bone through the slices.

Histological evaluation of the cranial defect

Tissue samples were harvested from the defect following terminal microCT imaging at week 12 and prepared for histology (n=3). Defect segments were decalcified, embedded in paraffin, and stored at −20 °C. Prior to antibody staining, paraffin sections were de-waxed in ethanol and xylene solutions, and 5-μm sections were obtained on a microtome. Sections were prepared for H&E and Masson's Trichrome staining. Immunofluorescence staining was performed for the following targets: CD68 (primary: anti-rat CD68 (ABD Serotec, Raleigh, NC); secondary: AlexaFluor 594 (Life Technologies, Carlsbad, CA)), CD29 (anti-rat Alexafluor 647 CD29 (Biolegend, San Diego, CA)), and CD90 (primary: anti-rat CD90 (Abcam, Cambridge, MA); secondary: Dylight 594 (Invitrogen)). Samples were incubated with primary antibody overnight at 4 °C, and secondary antibody for 1 h at room temperature with agitation. Images were acquired on a Zeiss LSM 700–405 confocal microscope (Zeiss, Thornwood, NY).

MICROFIL© analysis of vascularization in cranial defect

To assess vascular perfusion of the cranial defects in an independent study, rats treated with coated graft, control graft, or no graft were euthanized at week 2 and week 12 (n=3 per group per time point) and their vasculature was perfused with MICROFIL© (Flow Tech, Carver, MA) and imaged via microCT [12, 30, 31]. Briefly, rats were anesthetized with 2.5 % isoflurane gas and euthanized via intracardiac injection of pentobarbital (250 mg/kg), and the common carotid arteries were cannulated. The vasculature was flushed with 10 mL 2 % heparin-saline, then filled with 3 mL MICROFIL© injected simultaneously through both arteries, and allowed to set for 16 h at 4 °C. The top of the skull was harvested, fixed, and decalcified. The samples were scanned in air with the following parameters: 21-μm voxel size, 45 kVp, 177 μA, medium resolution, 21.5-mm-diameter field of view, 200-ms integration time, and threshold of 164–1500 mg HA/cm^3. Similar to bone analysis, 2D contours were drawn to enclose the area of interest, excluding the sagittal sinus because of its large volume compared to other microvasculature, and due to the large variance of its size between samples.

Statistical analysis

Data are presented as mean±s.e.m., and all statistical analyses were performed in GraphPad Prism 6. Bone volume and bone density in the cranial defect were compared between groups at each time point using unpaired *t* test. For mouse tibial fracture studies, $n=3$ per group per time point for each measurement was implemented. For rat cranial defect studies, $n=3$ per group per time point for each measurement was implemented.

Results

Local administration of FTY720 via ECM gel accelerates mouse tibial fracture repair

Tibial fractures treated with low and high doses of FTY720 show no significant difference but a trend of increasing bone volume compared to vehicle control at week 2 as measured by microCT (Fig. 1a). FTY720 appears to accelerate the formation and resolution of the fracture callous during the first 3 weeks, as indicated by the arrows in Fig. 1b. By week 4, tibias treated with low doses of FTY720 appear to achieve cortical union as indicated by representative microCT images and H&E staining (Fig. 1c, d).

Sustained release of FTY720 from human bone allograft

FTY720 was directly adsorbed to the surface of human donor trabecular bone allografts, as confirmed by fluorescence microscopy (Fig. 2a). Quantification of pre- and post-loading solutions indicated an average loading of 193 μg FTY720/mm^3 bone graft. FTY720 releases from the graft surface over the course of 1 week, with a burst release in the first 3 days and continued release over the remaining 4 days (Fig. 2c).

Release of FTY720 from human trabecular bone allograft accelerates bone deposition in rat cranial defect

The surface of semicircular mineralized human trabecular allograft was directly loaded with FTY720 and placed within a rat critical-sized cranial defect. Since new bone formation is necessary to heal the critical-sized defect, changes in bone volume and bone density were assessed via microCT at weeks 0, 2, 4, 6, 10, and 12. Defects treated with FTY720-coated grafts show significantly higher bone volume by week 6 and bone density by week 10 (Fig. 3a, b). Thus, direct adsorption of FTY720 to bone graft enhances osseous regeneration and engraftment potential. Bone volume shows an increasing trend for 12 weeks while bone density increases only until week 10, suggesting that bone deposition occurs preferentially outside the graft as opposed to within the graft. As shown in representative images in Fig. 3c, FTY720 enhances new bone deposition along the graft-host bone interface and in the void space.

Histological evaluation of osteogenesis and graft incorporation

Masson’s trichrome staining was used to assess the tissue composition of key regions in the cranial defect at week 12. Qualitative evaluation of the entire graft region suggests that FTY720 stimulates robust tissue growth into the graft compared to uncoated graft which contains large areas devoid of tissue (Fig. 4a). Host-derived osteoid was distinguished from graft-derived osteoid by the presence of pink cytoplasmic stain in regions of deep blue

collagen coloration. Both graft groups show graft-host bridging formed by a mixture of fibrous tissue and nascent osteoid (Fig. 4b). FTY720 appears to increase mature osteoid formation within the graft region and void region compared to control graft (Fig. 4c, d, *asterisks*). H&E staining confirms the observation that FTY720 augments tissue ingrowth into the graft (Fig. 5).

We have shown previously that local administration of FTY720 regulates the trafficking of inflammatory and osteogenic progenitor cells to sites of injury [9, 10, 32]. In order to assess the phenotype of cells recruited to the graft region, we performed immunohistochemical staining on defect tissue sections to visualize macrophages (CD68) and stromal populations enriched for osteogenic progenitor cells (CD29, CD90) [32]. As shown in Fig. 5, FTY720 appears to modestly reduce accumulation of $CD68^+$ macrophages and dramatically increase $CD29^+$ cell infiltration into the graft region, with mild effect on $CD90^+$ cell number.

Release of FTY720 from human trabecular bone allograft enhances early vascularization

Representative microCT images of MICROFIL© perfused animals show vascularity within the defect at weeks 2 and 12 (Fig. 6). FTY720 appears to increase vascular density within the graft relative to control at week 2 (Fig. 3a, b). By week 12, vasculature appears more extensive in the control (Fig. 6).

Discussion

By exploiting the growth factor sequestration and release properties of natural ECM, FTY720 was locally delivered to a mouse tibial fracture via Matrigel® injection and promoted limited bone regeneration at the injury site. During endochondral osteogenesis such as fracture healing, the first step is creation of a callous that provides temporary mechanical stability while osteogenic cells migrate into the defect to remodel the callous into bone and achieve cortical union between the two ends of the defect [33, 34]. A recent study observed that systemic treatment with FTY720 after tibial fracture in mice did not improve healing parameters [35], likely because the local effect of bone progenitor cell recruitment did not occur. We observe that callous formation and remodeling appear accelerated in FTY720-treated fractures (Fig. 1b). It has been shown that FTY720 enhances BMP-2-mediated osteoblast differentiation [36] and that FTY720 significantly enhances SDF-1α-mediated chemotaxis of bone marrow stromal cells [32], both of which could contribute regenerative cell populations to deposit and remodel the fracture callous.

We further exploited the ability of natural matrix to sequester and release FTY720 by coating the drug directly on the surface of human trabecular bone allograft, thus enabling investigation of an off-the-shelf, currently clinically used bone regeneration platform (allograft) with greater potential for clinical translation than polymer-based strategies. While in previous studies FTY720 release from cranial allograft was driven by degradation of the PLAGA vehicle, here drug release depends on diffusion from the surface of the mineralized bone matrix. We observe at least a 20-fold increase in FTY720 released from the directly coated bone grafts (43.0 μg at 7 days) compared to the PLAGA-coated grafts used previously (2.4 μg at 5 days), yet a smaller increase in bone volume [12]. It is possible that the dose of FTY720 in the present study exceeds the local concentration that optimally

promotes vascularization and bone regeneration [12, 16]. Healing outcomes may be improved in future studies by reducing the FTY720 payload on the graft surface. Furthermore, differential release kinetics between PLAGA and direct adsorption strategies must be considered, since FTY720 released during PLAGA bulk degradation at later weeks may contribute to regeneration. In the PLAGA-coated allograft, FTY720 loading was limited by its saturation limit in PLAGA solution prior to coating the graft; here FTY720 loading is limited primarily by the surface area of the graft itself, which may allow for the higher loading efficiency. We speculate that electrostatic interactions between the FTY720 molecule, specifically the H+ that transiently associates with the amine group (critical micelle concentration of FTY720 + H+ = 75 μM) [37, 38], and the slight negative charge of bone surface [39], are responsible for FTY720 binding to the human allograft bone matrix (Fig. 2b). Estimating the size of the FTY720 molecule to be 2900 $Å^3$ using lipid parameters (calculated from [40]), theoretically, the bone surface can bind up to 7.9E10 FTY720 molecules/mm^2 (Fig. 2b). Release continues for 1 week (Fig. 2c), enabling sustained bioactivity of FTY720 in the wound healing environment. This loading strategy could be tuned in future studies by varying the initial drug concentration in the loading solution to create shorter release times at lower doses.

Histological evaluation of the cranial defect corroborates evidence of enhanced bone formation assessed by microCT. H&E staining shows robust tissue ingrowth into FTY720-coated grafts, and Masson's trichrome staining suggests that FTY720 enhances osteoid formation in the graft and void regions (Fig. 4c, d). The effectiveness of FTY720 in this study may result from effects on inflammatory and osteogenic cell recruitment. Current understanding of the inflammatory cascade during wound healing suggests that both magnitude and phenotype of immune cell infiltration regulate healing outcomes [9, 10, 41]. Previous studies have shown that FTY720 enhances the recruitment of anti-inflammatory monocytes [9] and M2-like macrophages [10] associated with wound healing. Enhanced bone regeneration observed in FTY720-treated defects in the present study (Figs. 3 and 4) may be influenced by reduced inflammatory response, as evidenced by reduced $CD68^+$ macrophage accumulation (Fig. 5), or possibly a skewing of the population toward M2-like phenotypes. We stained for markers indicative of osteogenic progenitor cell populations and observed a higher frequency of $CD29^+$ cells within FTY720-coated grafts, possibly indicating enhanced recruitment of endogenous progenitor cells to sites of new bone formation.

It is well documented that bone graft survival depends on host integration through neovascularization and bone graft resorption [42, 43]. In a clinical trial using a rh-BMP2-releasing sponge in human tibial fractures, 23 % of human subjects experienced treatment failure due to lack of graft integration [44]. Previous work has shown that FTY720 promotes growth of vascular networks when locally applied in a mouse dorsal skinfold window chamber [13, 14] and within cranial defect models [12, 16]. Vascular penetration into the graft reduces necrosis and ischemia thereby improving graft integration [45]. Here, we show that FTY720 released directly from the graft surface appears to increase vascularization within the graft at week 2 (Fig. 6), which may contribute to accelerated bone formation observed by weeks 6 and 10 (Fig. 3a, b). By week 12, accelerated osteoid formation in the FTY720-treated defect may cause attenuation of the vascular network and thereby decrease

vascular density compared to control. Although FTY720-treated defects do not have greater vascular investment and new bone deposition at week 12, the observed acceleration of these processes is likely to enhance graft performance, as Mah et al. showed that the rate of graft incorporation determines the efficacy of FDA-approved alloplastic bone materials in rat cranial defects [46]. Taken together, this study suggests that bone matrix binding of FTY720 may be used to direct bone allograft incorporation.

Conclusion

This study explored the use of natural ECM to sequester and release a sphingolipid growth factor (FTY720) to promote endogenous bone repair. This study provides preliminary evidence that local delivery of FTY720 via ECM gels or direct binding to human bone allografts may enhance healing outcomes in rodent models of tibial fracture and a critical-sized cranial defect, respectively. Removal of the polymer component of the drug delivery system in favor of ECM binding may potentially increase clinical translatability of this technology and further improve mineralized bone allograft incorporation and long-term graft survival.

Acknowledgments

This work was supported by NIH R01 DE019935 and NIH R01 AR056445.

References

1. Jacobs J, Andersson G, Bell J-E, Weinstein S, Dormans J, Gnatz S, Lane N, Puzas J, StClair EW, Yelin E. The burden of musculoskeletal diseases in the United States. Am Acad Orthop Surg. 2008
2. Jahangir A, Nunley R, Mehta S, Sharan A. Bone-graft substitutes in orthopaedic surgery, in AAOS Now. Am Acad Orthop Surg. 2008
3. Giannoudis PV, Dinopoulos H, Tsiridis E. Bone substitutes: an update. Injury. 2005; 36(Suppl 3):S20–7. [PubMed: 16188545]
4. Summers BN, Eisenstein SM. Donor site pain from the ilium. A complication of lumbar spine fusion. J Bone Joint Surg (Br). 1989; 71(4):677–80. [PubMed: 2768321]
5. Delloye C, et al. Bone allografts: what they can offer and what they cannot. J Bone Joint Surg (Br). 2007; 89(5):574–9. [PubMed: 17540738]
6. Wheeler DL, Enneking WF. Allograft bone decreases in strength in vivo over time. Clin Orthop Relat Res. 2005; 435:36–42.
7. Wu N, et al. Health care utilization and costs in patients experiencing bone fracture nonunion. Value Health. 2012; 15(4):A66.
8. Wieghaus KA, et al. Small molecule inducers of angiogenesis for tissue engineering. Tissue Eng. 2006; 12(7):1903–13. [PubMed: 16889520]
9. Awojoodu AO, et al. Sphingosine 1-phosphate receptor 3 regulates recruitment of anti-inflammatory monocytes to microvessels during implant arteriogenesis. Proc Natl Acad Sci U S A. 2013; 110(34): 13785–90. [PubMed: 23918395]
10. Das A, et al. The promotion of mandibular defect healing by the targeting of S1P receptors and the recruitment of alternatively activated macrophages. Biomaterials. 2013; 34(38):9853–62. [PubMed: 24064148]
11. Das A, et al. Delivery of S1P receptor-targeted drugs via biodegradable polymer scaffolds enhances bone regeneration in a critical size cranial defect. J Biomed Mater Res A. 2014; 102(4): 1210–8. [PubMed: 23640833]
12. Huang C, et al. Local delivery of FTY720 accelerates cranial allograft incorporation and bone formation. Cell Tissue Res. 2012; 347(3):553–66. [PubMed: 21863314]

13. Sefcik LS, et al. Sustained release of sphingosine 1-phosphate for therapeutic arteriogenesis and bone tissue engineering. Biomaterials. 2008; 29(19):2869–77. [PubMed: 18405965]
14. Sefcik LS, et al. Selective activation of sphingosine 1-phosphate receptors 1 and 3 promotes local microvascular network growth. Tissue Eng A. 2011; 17(5–6):617–29.
15. Brinkmann V, et al. Fingolimod (FTY720): discovery and development of an oral drug to treat multiple sclerosis. Nat Rev Drug Discov. 2010; 9(11):883–97. [PubMed: 21031003]
16. Petrie Aronin CE, et al. FTY720 promotes local microvascular network formation and regeneration of cranial bone defects. Tissue Eng A. 2010; 16(6):1801–9.
17. Semete B, et al. In vivo evaluation of the biodistribution and safety of PLGA nanoparticles as drug delivery systems. Nanomedicine. 2010; 6(5):662–71. [PubMed: 20230912]
18. Shive MS, Anderson JM. Biodegradation and biocompatibility of PLA and PLGA microspheres. Adv Drug Deliv Rev. 1997; 28(1):5–24. [PubMed: 10837562]
19. Ji W, et al. Biocompatibility and degradation characteristics of PLGA-based electrospun nanofibrous scaffolds with nanoapatite incorporation. Biomaterials. 2012; 33(28):6604–14. [PubMed: 22770568]
20. Lu JM, et al. Current advances in research and clinical applications of PLGA-based nanotechnology. Expert Rev Mol Diagn. 2009; 9(4):325–41. [PubMed: 19435455]
21. Makadia HK, Siegel SJ. Poly Lactic-co-Glycolic Acid (PLGA) as biodegradable controlled drug delivery carrier. Polymers (Basel). 2011; 3(3):1377–97. [PubMed: 22577513]
22. Dennis SC, et al. Endochondral ossification for enhancing bone regeneration: converging native extracellular matrix biomaterials and developmental engineering in vivo. Tissue Eng B Rev. 2014; 21(3):247–66.
23. Benders KEM, et al. Extracellular matrix scaffolds for cartilage and bone regeneration. Trends Biotechnol. 2013; 31(3):169–76. [PubMed: 23298610]
24. Singelyn JM, et al. Naturally derived myocardial matrix as an injectable scaffold for cardiac tissue engineering. Biomaterials. 2009; 30(29):5409–16. [PubMed: 19608268]
25. Sreejit P, Verma RS. Natural ECM as biomaterial for scaffold based cardiac regeneration using adult bone marrow derived stem cells. Stem Cell Rev Rep. 2013; 9(2):158–71.
26. Neal RA, et al. Alignment and composition of laminin-polycaprolactone nanofiber blends enhance peripheral nerve regeneration. J Biomed Mater Res A. 2012; 100A(2):406–23.
27. Hastings CL, et al. Drug and cell delivery for cardiac regeneration. Adv Drug Deliv Rev. 2014; 84:85–106. [PubMed: 25172834]
28. Tang PH, et al. Effective and sustained delivery of hydrophobic retinoids to photoreceptors. Invest Ophthalmol Vis Sci. 2010; 51(11):5958–64. [PubMed: 20574023]
29. Wallace DG, Rosenblatt J. Collagen gel systems for sustained delivery and tissue engineering. Adv Drug Deliv Rev. 2003; 55(12):1631–49. [PubMed: 14623405]
30. Butcher JT, et al. Quantitative volumetric analysis of cardiac morphogenesis assessed through micro-computed tomography. Dev Dyn. 2007; 236(3):802–9. [PubMed: 17013892]
31. Savai R, et al. Evaluation of angiogenesis using micro-computed tomography in a xenograft mouse model of lung cancer. Neoplasia. 2009; 11(1):48–56. [PubMed: 19107231]
32. Das A, et al. Delivery of bioactive lipids from composite microgel-microsphere injectable scaffolds enhances stem cell recruitment and skeletal repair. PLos One. 2014; 9(7)
33. Bax BE, Wozney JM, Ashhurst DE. Bone morphogenetic protein-2 increases the rate of callus formation after fracture of the rabbit tibia. Calcif Tissue Int. 1999; 65(1):83–9. [PubMed: 10369739]
34. McKibbin B. The biology of fracture healing in long bones. J Bone Joint Surg (Br). 1978; 60 B(2): 150–62. [PubMed: 350882]
35. Heilmann A, et al. Systemic treatment with the sphingosine-1-phosphate analog FTY720 does not improve fracture healing in mice. J Orthop Res. 2013; 31(11):1845–50. [PubMed: 23818033]
36. Sato C, et al. Sphingosine 1-phosphate receptor activation enhances BMP-2-induced osteoblast differentiation. Biochem Biophys Res Commun. 2012; 423(1):200–5. [PubMed: 22659743]
37. Bertran CA, Bertazzo S, Faria LP. Surface charge of hydroxyapatite and bone mineral. Bioceramics (19). 2007; 330–332(1 and 2):713–716.

38. Swain J, et al. Study of aqueous phase aggregation of FTY720 (fingolimod hydrochloride) and its effect on DMPC liposomes using fluorescent molecular probes. Phys Chem Chem Phys. 2013; 15(41):17962–70. [PubMed: 24048224]

39. Eriksson C, Jones S. Bone-mineral and surface-charge. Clin Orthop Relat Res. 1977; 128:351–3.

40. Kitagawa S, Sawada M, Hirata H. Fluorescence analysis with diphenylhexatriene and its ionic derivatives of the fluidity of liposomes constituted from stratum-corneum lipids - contribution of each lipid component and effects of long-chain unsaturated fatty-acids. Int J Pharm. 1993; 98(1–3):203–8.

41. Shechter R, et al. Infiltrating blood-derived macrophages are vital cells playing an anti-inflammatory role in recovery from spinal cord injury in mice. Plos Med. 2009; 6(7)

42. Zhang XP, et al. Periosteal progenitor cell fate in segmental cortical bone graft transplantations: implications for functional tissue engineering. J Bone Miner Res. 2005; 20(12):2124–37. [PubMed: 16294266]

43. Yu HY, et al. Improved tissue-engineered bone regeneration by endothelial cell mediated vascularization. Biomaterials. 2009; 30(4):508–17. [PubMed: 18973938]

44. Golden JD, et al. Recombinant human BMP-2 and allograft compared with autogenous bone graft for reconstruction of diaphyseal tibial fractures with cortical defects. J Bone Joint Surg Am Vol. 2008; 90A(5):1168–9.

45. Koffler J, et al. Improved vascular organization enhances functional integration of engineered skeletal muscle grafts. Proc Natl Acad Sci U S A. 2011; 108(36):14789–94. [PubMed: 21878567]

46. Mah J, et al. The efficacy of various alloplastic bone grafts on the healing of rat calvarial defects. Eur J Orthod. 2004; 26(5):475–82. [PubMed: 15536835]

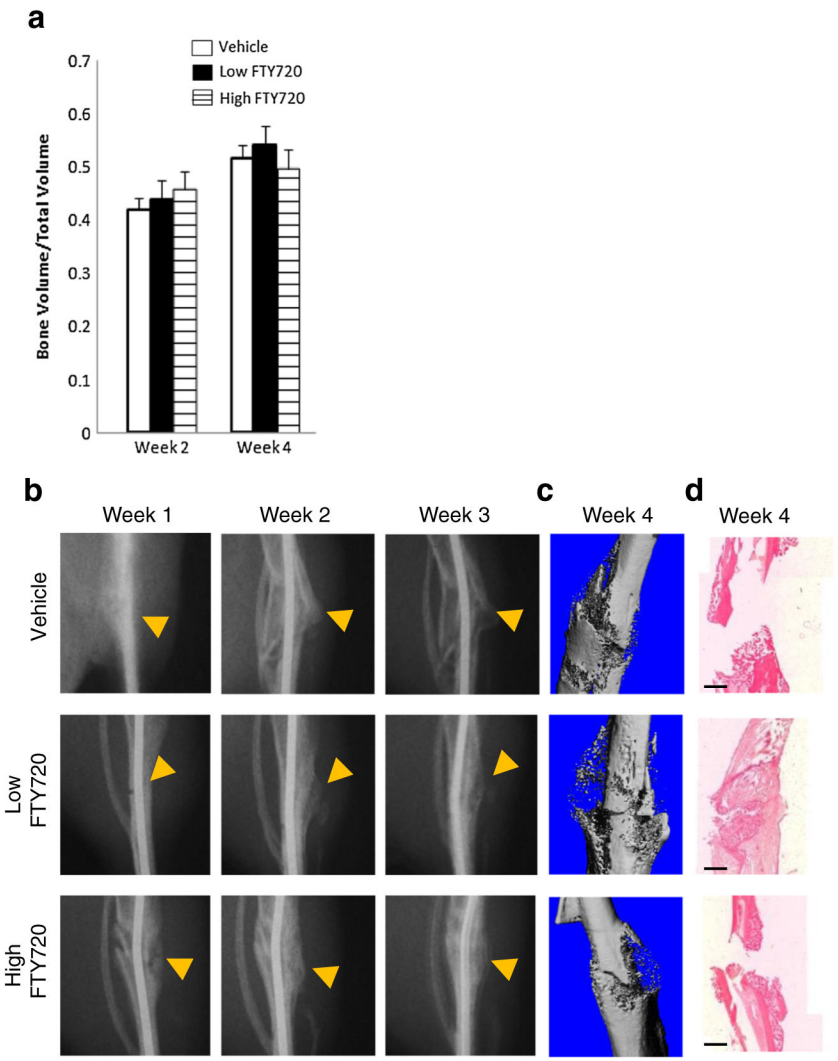

Fig. 1.

FTY720 released from Matrigel® accelerates callous remodeling in mouse tibial defect. **a** Bone volume to total volume ratio evaluated by microCT in the mouse tibial defect (n=3 per time point). **b** Representative X-ray images of defect healing and callous remodeling from weeks 1–3. *Arrow* indicates location of fracture and callous. MicroCT reconstruction (**c**) and H&E histological staining (**d**) of excised tibia at week 4. *Scale bar* = 500 μm

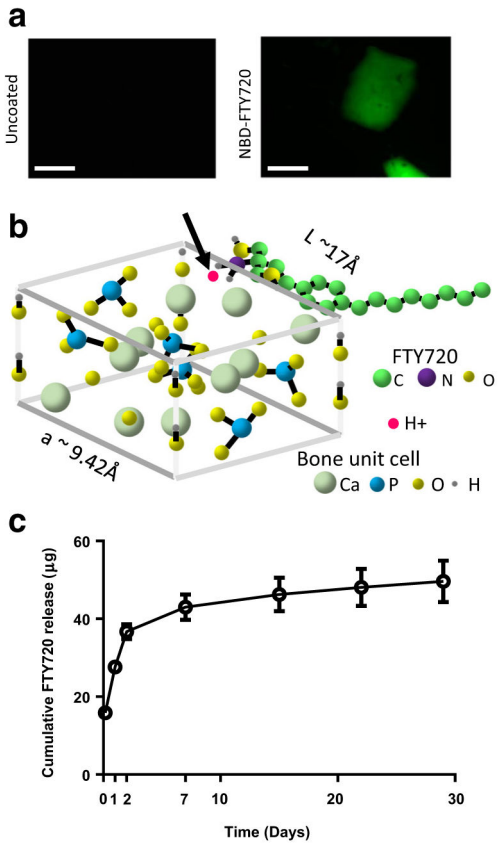

Fig. 2.

FTY720 binding to allograft bone. **a** Fluorescence microscopy of bone chips coated with NBD-labeled FTY720 as per methods. Bone chips without FTY720 show no signal (*scale bar*=1 mm). **b** Potential mechanism by which FTY720 binds to bone, via a transiently associated H+ (indicated by *red dot* and *black arrow*) to the NH2 group on the drug molecule interacting with the negatively charged bone surface. **c** Release of FTY720 from the bone graft surface is sustained for 1 week (n=6). *Scale bar* = 500 µm (Color figure online)

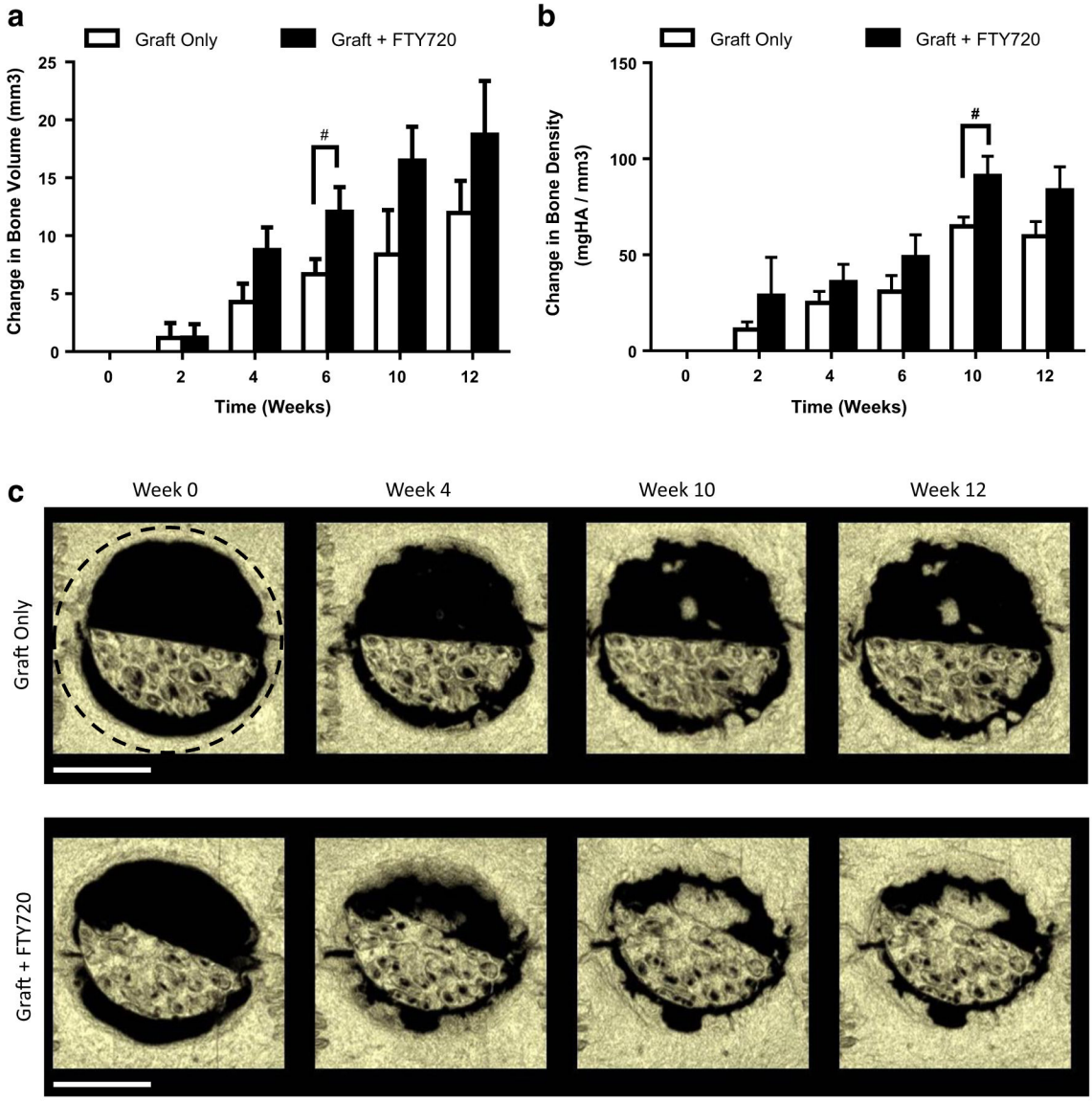

Fig. 3.

FTY720 released from the surface of human trabecular bone allograft accelerates bone regeneration. FTY720-treated defects have greater **a** bone volume at week 6 and **b** bone density at week 10. **c** Representative microCT reconstructions of rat cranial defects implanted with FTY720-coated human trabecular allografts. The region of quantification is indicated by the *black dashed circle*. #p<0.1 compared to graft only by unpaired t test (n=3). *Scale bar* = 4 mm

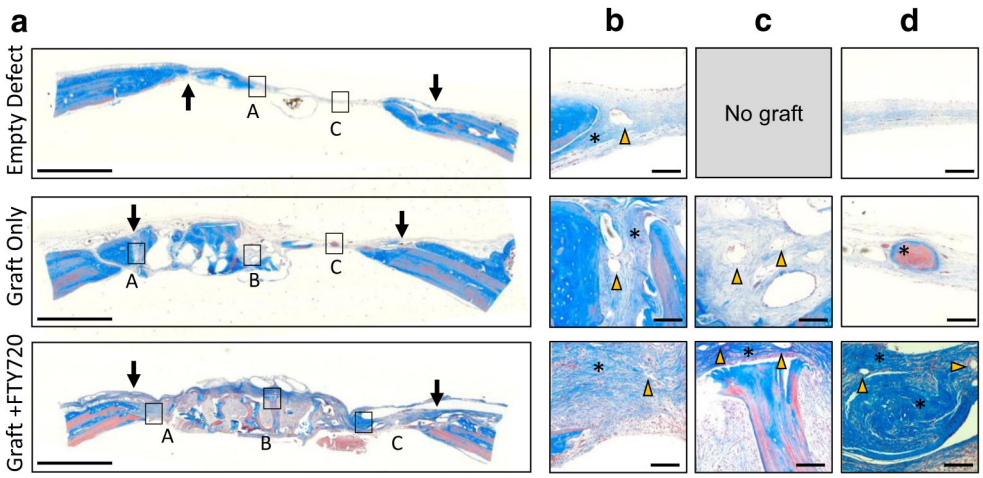

Fig. 4.

Representative Masson's trichrome staining of human trabecular bone graft in rat cranial defect at 12 weeks. The edge of the defect is indicated by *arrows* in (**a**). Insets show **b** bridging region between graft and host bone, **c** graft region, and **d** tissue formed in the void space. The empty defect has no graft image as no graft was implanted. *Yellow arrows* indicate blood vessels and *asterisks* indicate osteoid deposited by the host. *Scale bar* in (**a**) = 2 mm; *scale bar* in (**b**–**d**) = 100 μm (Color figure online)

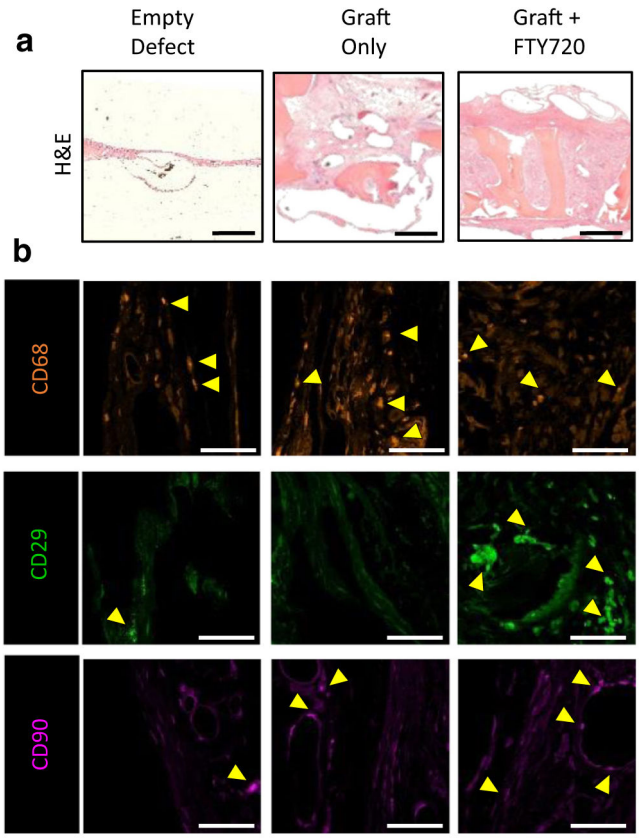

Fig. 5.

Histological evaluation of the graft region at 12 weeks. **a** H&E staining reveals extensive tissue growth into the FTY720-coated graft. **b** Representative images of immunohistochemical staining for CD68 (macrophages) and CD29 and CD90 (bone progenitors) in the graft region reveals decreased macrophage and increased bone progenitor infiltration into FTY720-coated graft. *Scale bar* in (**a**) = 500 μm; *scale bar* in (**b**) = 50 μm

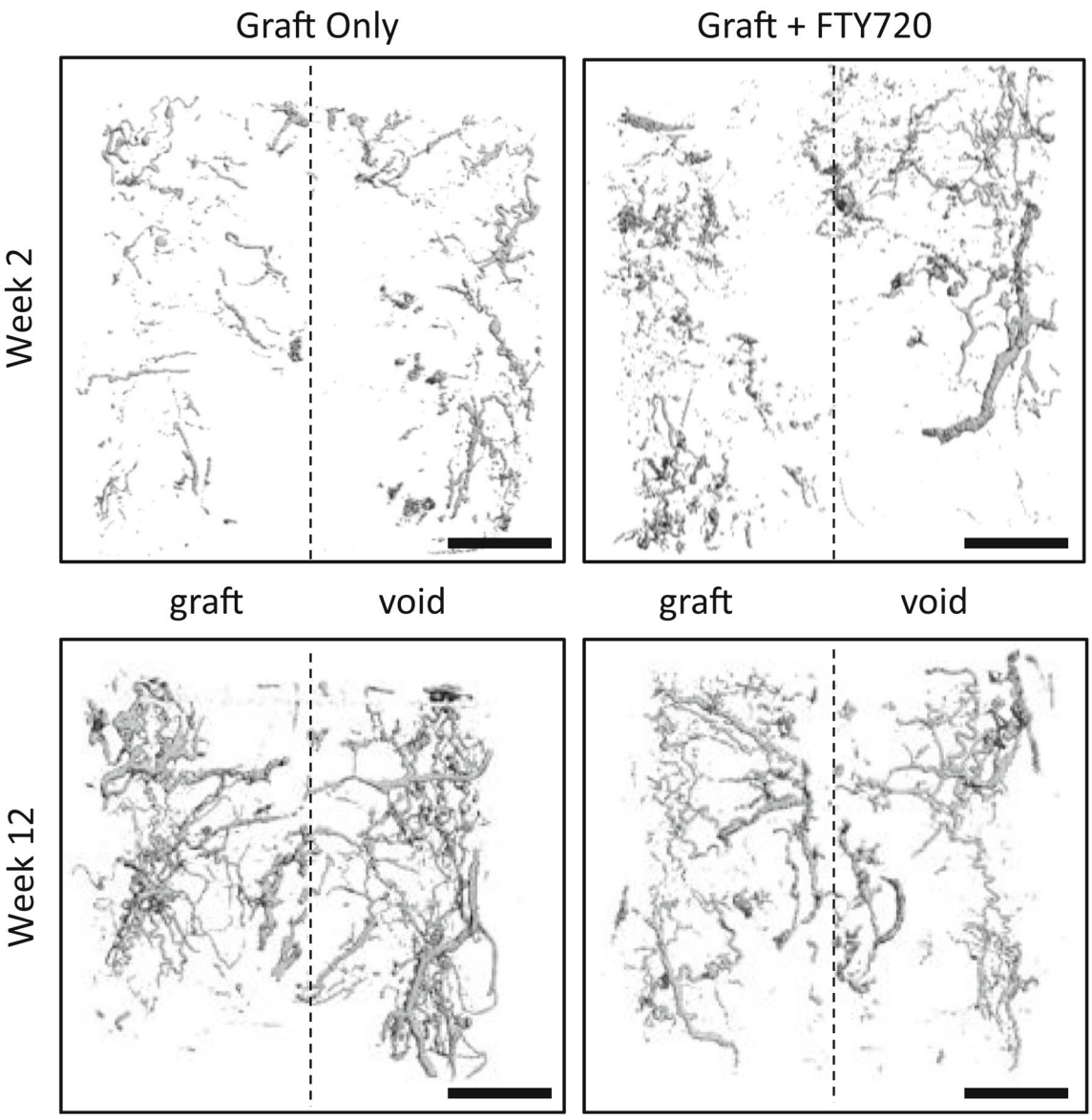

Fig. 6.

FTY720 released from human trabecular bone allograft accelerates vascularization of the graft. Representative MicroCT imaging of MICROFIL© perfused animals reveals higher vascular density within FTY720-treated grafts by week 2 but not week 12. *Scale bar* = 2 mm